PCCP

Accepted Manuscript

ROYAL SOCIETY OF CHEMISTRY

www.rsc.org/pccp

Journal Name

RSCPublishing

ARTICLE

Consequences of CO_2 solubility for hydrate formation from carbon dioxide containing water and other impurities

Cite this: DOI: 10.1039/x0xx00000x

Received 00th January 2012,
Accepted 00th January 2012

DOI: 10.1039/x0xx00000x

www.rsc.org/

Bjørn Kvamme[a], Tatiana Kuznetsova[a], Bjørnar Jensen[a], Sigvat Stensholt[a], Jordan Bauman[a], Sara Sjøblom[a], and Kim Nes Lervik[a],

Deciding on the upper bound of water content permissible in a stream of dense carbon dioxide under pipeline transport conditions without facing the risks of hydrate formation is a complex issue. In this work, we outline and analyze ten primary routes of hydrate formation inside a rusty pipeline, with hydrogen sulfide, methane, argon, and nitrogen as additional impurities. A comprehensive treatment of equilibrium absolute thermodynamics as applied to multiple hydrate phase transitions is provided. We also discuss in detail the implications of the Gibbs phase rule that make it necessary to consider non-equilibrium thermodynamics. The analysis of hydrate risk has been revised for the dominant routes, including the one traditionally considered in industrial practice and hydrate calculators. The application of absolute thermodynamics with parameters derived from atomistic simulations lead us to several important conclusions regarding the impact of hydrogen sulfide. When present at studied concentrations below 5 mol%, the presence of hydrogen sulfide will only support the carbon-dioxide-dominated hydrate forming on the phase interface from liquid water and hydrate formers entering from the carbon dioxide phase. This is in contrast to a homogeneous hydrate nucleation and growth inside the aqueous solution bulk. Our case studies indicate that hydrogen sulfide at higher than 0.1 mol% concentration in the carbon dioxide can lead to growth of multiple hydrate phases immediately adjacent to the adsorbed water layers. We conclude that hydrate formation via water adsorption on rusty pipeline walls will be the dominant contributor to the hydrate formation risk, with initial concentration of hydrogen sulfide being the critical factor.

Introduction

Pipeline transport of large volumes of carbon dioxide at low temperatures and high pressures has recently become a topic of relevance due to the growing number of projects that will require carbon dioxide to be delivered to its underground storage destination. Under these conditions, carbon dioxide has been known to aggressively form crystalline ice-like compounds, so-called clathrate hydrates [1 and references therein]. Traditionally, the hydrate risk evaluation has been based on straightforward dew-point calculations despite the fact that rusty pipeline walls will make for excellent sites for water adsorption and thus add additional pathways for hydrate formation. The formation of hydrate inside a stream of dense carbon dioxide will pose a complex problem involving several phase transitions with competing mechanisms and pathways, with the outcome ultimately depending on the details of thermodynamics and kinetics of processes involved. This work focused on transport of carbon dioxide with impurities, with water and hydrogen sulfide acting as the additives.

Hydrates forming from water and hydrate formers in a pipeline will generally unable to reach thermodynamic equilibrium for several reasons. In the simplest case of carbon dioxide hydrate forming directly from water dissolved in carbon dioxide, there would be two components C (water and carbon dioxide) and two phases $N = 2$ (solid hydrate and dense carbon dioxide with impurities). The number of degrees of freedom F would therefore be two according to the Gibbs phase rule ($F = C - N + 2$), indicating a possibility to reach equilibrium due to local temperature and pressure representing the two degrees of freedom. Since the water concentration in carbon dioxide will be very limited, this possibility of hydrate formation might not present a practical problem due to the inherent limitations on mass transport needed to assemble hydrate crystals.

The presence of solid surfaces will raise yet another question of whether the creation of fluid phases should be considered independent of hydrate formation. Water wetting solid surfaces provides excellent nucleation sites for efficient heterogeneous hydrate formation, and their impact cannot be discounted by arguments that the gas phase would dominate the phase transition because of its dominance in mass. More specifically, the two main hydrate formation routes will both be impacted by the effect of solid surfaces given that water dissolved in carbon dioxide will readily adsorb on the rusty pipeline walls. Hydrate can then start forming either from water and hydrate formers which are both adsorbed on the surface or from adsorbed water and hydrate formers transported from the fluid phase. In a non-equilibrium situation, the chemical potentials of different components will vary from one phase to another, thus hydrate growing in different phases will have different free energies, as indicated by statistical thermodynamics hydrate models [1]. Thus even the simplest scenario that only involves dissolved water could result in formation of several different co-existing hydrate phases.

Alternative pathways to hydrate formation: the impact of multiple phases

In a more complicated case of case of two components (carbon dioxide and water) and four possible phases (carbon dioxide fluid, liquid water, adsorbed phase, hydrate) discussed above, the Gibbs phase rule will indicate zero degrees of freedom. The system will be over-determined by two independent thermodynamic variables since temperature and pressure will be locally defined through coupling to fluid dynamics and heat transport dynamics. One could argue that that adding two components to the fluid phase would change the situation and allow the system to achieve equilibrium. However, the combination of the first and the second law of thermodynamics will direct the system to the state of lower free energy currently possible in the specific region. This would lead to the most stable hydrates forming first, and the initial hydrate being dominated by hydrogen sulfide, a much better hydrate former than carbon dioxide. As the result, the composition of the forming hydrate will vary over time, with the corresponding gradual change in hydrate free energy. From the thermodynamic point of view, these hydrates of varying composition and density will constitute separate phases, complicating the application of the Gibbs phase rule even further. A more stable hydrate will be unable to reform into a less stable form due to the laws of thermodynamics, while a less stable hydrate would be unable reform into a more stable one without an access to new hydrate formers that would increase its stability. Under continuous flow, the latter option may become feasible due to continuous supply of "fresh" components passing by. In addition, when in contact with phases under-saturated with respect to hydrate formers, hydrate may also dissolve, as well as reform with different compositions. From a dynamic point of view, it is however unlikely that any state of hydrate equilibrium can be reached during the pipeline transport of carbon dioxide with impurities.

Table 1 below systemizes the important alternative routes to hydrate formation and possible re-dissociation based on free energy changes associated with the phase transitions:

$$\Delta G_i = \delta\left[x_w^{H,i}(\mu_w^{H,i} - \mu_w^{p}) + x_{gas}^{H,i}(\mu_{gas}^{H,i} - \mu_{gas}^{p}) \right] \quad (1)$$

Where H denotes the hydrate phase, i represents any of the ten phase transition scenarios, p indicates liquid, gas and adsorbed phases, x composition and μ chemical potential. δ is equal to 1 for hydrate formation or reformation and -1 for dissociation. One should keep in mind that hydrates created along the pathways in Table 1 will also differ in filling fractions and corresponding different free energies, thus each hydrate forming process will result in a unique phase.

Table 1. Potential hydrate phase transition scenarios for a system of carbon dioxide with impurities relevant for pipeline transport. The free energy change calculated following equation 1 for all the processes. Note that different phase transitions may involve hydrate of different composition and thus the label hydrate for the phase does not distinguish between different hydrate free energies.

i	δ	Initial phase(s)	Driving force	Final phase(s)
1	-1	Hydrate	Outside stability in terms of local P and/or T	Gas, Liquid water
2	-1	Hydrate	Sublimation (gas under saturated with water)	Gas
3	-1	Hydrate	Outside liquid water under saturated with respect to carbon dioxide and/or other enclathrated impurities originating from the carbon dioxide phase	Liquid water, (Gas)
4	-1	Hydrate	Hydrate gets in contact with solid walls at which adsorbed water have lower chemical potential than hydrate water	Liquid water, Gas
5	+1	Gas/fluid	Hydrate more stable than water and hydrate formers in the fluid phase	Hydrate
6	+1	Gas + Liquid water	Hydrate more stable than condensed water and hydrate formers from gas/fluid	Hydrate
7	+1	Surface reformation	Non-uniform hydrate rearranges due to mass limitations (lower free energy hydrate particles consumes mass from hydrates of higher free energy)	Hydrate
8	+1	Aqueous Phase	Liquid water super saturated with carbon dioxide and/or other hydrate formers, with reference to hydrate free energy	Hydrate
9	+1	Adsorbed	Adsorbed water on rust forms hydrate with adsorbed hydrate formers.	Hydrate
10	+1	Adsorbed +fluid	Water and hydrate formers from gas/fluid forms hydrate	Hydrate

Schemes used at present in industrial hydrate risk evaluation are predominantly based on formation of hydrate from gas and liquid water (route 6), with pressure and temperature projection of the phase stability boundaries used for to assess the risks. In practice, this approach involves estimating the limits for water dropout from the fluid carbon dioxide phase and subsequent evaluation of hydrate equilibrium in terms of pressure and temperature alone. Few (if any) commercial and academic codes that are openly available are capable of evaluating homogeneous hydrate formation from solution of hydrate formers dissolved in water. There are no available hydrate codes capable of handling heterogeneous hydrate formation influenced by presence of solid surfaces. The lack of such tools turns into an important omission due to the growing evidence of hydrate films dominated by growth on surfaces, even in absence of flow. In this sense, this paper could also contribute to stimulating the discussion on how to incorporate these aspects [2, 6] into the new generation of hydrate risk evaluation tools based on non-equilibrium thermodynamics. This analysis could also be extended to the transport of hydrocarbons or other hydrate-forming fluids containing water.

The more rigorous approach to hydrate risk evaluation In view of Table 1 would involve developing a scheme for free energy minimization that will also incorporate mass and heat transport as the minimum constraints. Hydrodynamic effects will also need to be included in cases where rapid dissociation will result in formation of separate fluid phases upon the release of hydrate formers. Simpler but less rigorous analysis which is more directly compatible with conventional hydrate equilibrium numerical codes will be another viable alternative, provided that consistent absolute thermodynamic properties are available for the different phase transitions. For example, either the classical nucleation theory or the Multi-component Diffuse Interface Theory (MDIT) [2, 3] can be used to evaluate the phase transitions in Table 1. Phase transitions associated with either a positive free energy changes or a change not negative enough to overcome the penalty of work on the surrounding will not occur and can be eliminated out of hand, such will be the case of routes 1 through 4. Simple theories can be used to exclude very slow phase transitions and thus allow one to focus the evaluation on a handful of really important phase transitions.

Providing routes to absolute (ideal gas as reference state) thermodynamic properties for all co-existing phases is also an important aspect of this paper. Models used may be refined and extended further but the approach presented here provides a good starting point for an accurate analysis of hydrate formation thermodynamics. For this purpose, as well as for model verification, a section on equilibrium thermodynamics is presented next. A brief discussion of implications imposed by the largely non-equilibrium nature of processes encountered during hydrate phase transitions follows. The subsequent sections are devoted to numeric modelling focusing on evaluating the possible routes to hydrate formation by utilizing equation (1). This approach requires the application of absolute thermodynamics for all of the phases; absolute thermodynamic properties derived from molecular-level simulations have been proven to predict hydrate equilibrium curves quite well [1, 2].

Equilibrium thermodynamics

Formally, a thermodynamic equilibrium is achieved when the temperatures, pressures and chemical potentials of all co existing phases are uniform across all phase boundaries. It might however be convenient to start with an alternative formulation of chemical potential of a component *i*, μ_i, in terms of fugacity, fi, for the same component.

$$d\mu_i = RTd\ln f_i \quad (2)$$

With ideal gas as reference the limits of (2) is defined as:
$\lim(f_i) = y_i P$ when $P \to 0$ (3)
and

$$\mu_i(T,P,\vec{y}) - \mu_i^{ideal\,gas}(T,P,\vec{y}) = RT\ln\frac{f_i(T,P,\vec{y})}{y_i P} = RT\ln\phi_i(T,P,\vec{y}) \quad (4)$$

where ϕ_i is the fugacity coefficient for component *i* in a given phase.

As an intermediate step, another reference state for fugacity of a component *i* in liquid state will also be used:

$$\mu_i(T,P,\vec{x}) - \mu_i^{idealliquid}(T,P,\vec{x}) = RT\ln\frac{f_i(T,P,\vec{x})}{x_i f_i^{pureliquid}(T,P)} = RT\ln\gamma_i(T,P,\vec{x}) \quad (5)$$

$$\lim(\gamma_i) = 1.0 \quad \text{when } x_i \to 1.0$$

where γ_i is the activity coefficient for component i in the liquid mixture. The corresponding fugacity formulation can be expressed in the following fashion:

$$f_w^{Liquid}(T,P,\vec{x}) = x_w\gamma_w(T,P,\vec{x})\phi_w^{puregas}(T,P_w^{sat})P_w^{sat}(T)e^{\int_{P_i^{sat}}^{P}\frac{\bar{v}_i}{RT}dP} \quad (6)$$

which makes use of the equilibrium between pure gas and pure liquid at the vapor pressure curve:

$$f_w^{pureliquid}(T) = f_w^{puregas}(T) = \phi_w^{puregas}(T,P_w^{sat})P_w^{sat} \quad (7)$$

and integration back to the actual pressure at constant temperature using the pressure dependency of chemical potential for water will yield

$$d\mu_w^{pureliquid}(T,P) = RTd\ln f_w^{pureliquid}(T,P) = \bar{v}_w(T,P)dP \quad (8)$$

where $\bar{v}_w(T,P)$ is the molar volume of pure liquid water. When integrated and used in equation (6), it will yield the so-called Poynting correction that accounts for the difference between the saturated pressure corresponding to a given T and the actual pressure. The low molar volume of water results in the Poynting correction being close to unity for a wide range of pressures.

Yet another reference state is useful when the concentration of gasses dissolved in water is low, as will be the case of route 8:

$$\mu_i(T,P,\vec{x}) - \mu_i^{\infty}(T,P,\vec{x}) = RT\ln\left[x_i\gamma_i^{\infty}(T,P,\vec{x})\right] \quad (9)$$

$$\lim(\gamma_i^{\infty}) = 1.0 \quad \text{when } x_i \to 0 \quad (10)$$

where the ∞-superscript denotes infinite dilution solution. This particular convention is denoted as the non-symmetric convention since the limit of the activity coefficient in this case goes to unity for the component i is when the mole-fraction approaches zero. The corresponding fugacity formulation under this convention can be writes as follows:

$$f_i(T,P,\vec{x}) = x_i\gamma_i^{\infty}(T,P,\vec{x})f_i^{\infty}(T,P_0)\exp\left(\int_{P_0}^{P}\frac{\overline{v}_i^{\infty}(T,P,\vec{x})}{RT}dP\right) \quad (11)$$

where the subscript 0 on pressure denotes a reference pressure, often chosen as 1 bar for convenience, and the Poynting correction follows similar to (6) but now involves the partial molar volume for component i in the solvent at infinite dilution. The reference fugacity coefficient $f_i^{\infty}(T,P_0)$ can be back-calculated from extrapolations of experimental data.

Provided that thermodynamic properties of all phases can also be specified and evaluated outside of equilibrium, the first and second laws of thermodynamics would require that the available mass of each component, and the total mass, should be distributed over all possible phases able to coexist under the given local pressure and temperature conditions. This evaluation will be fairly straightforward for most of the fluid phases under consideration. The only phase that would require a special attention is the hydrate phase, which is point discussed extensively in Kvamme et.al. [2]. Combining thermodynamic formulations for fluids in equations (1) to (11) with hydrate non-equilibrium formulations from Kvamme et.al. [2] will make it fairly straightforward to minimize the free energy and obtain estimates for local phase distributions obeying the first and the second law of thermodynamics. Several algorithms capable of implementing this approach are available in the open literature.

From an industrial point of view, the risk of hydrate formation, and possible strategies to prevent hydrate from forming, is more interesting than the local distribution of all possible phases. Within this paper we will therefore discuss a more sequential analysis which would involve simple extensions of the hydrate evaluation tools available.

Most of the actual region of pressures and temperatures are in liquid state. The situations considered here imply very limited solubility and/or limited concentrations. Solubility of H_2O in CO_2 is very small. In view of this the following approximation should be sufficiently accurate for that case:

$$\mu_{i,j}(T,P,\vec{x}) \approx \mu_{i,j}^{\infty}(T,P) + RT\ln x_{i,j} + RT\ln\gamma_{i,j}^{\infty}(T,P,\vec{x}) \quad (12)$$

where subscript *j* denotes the component and *i* denotes the phase. In the context of this work, *j* is "CO_2" for the CO_2 phase, "H_2O" is the aqueous phase, "ads" is the phase adsorbed on hematite, and "H" is the solid hydrate phase.

Route 5: Formation of hydrate from dissolved water and impurities in carbon dioxide

This alternative route has been investigated by Kvamme et.al. [2] for water dissolved into the bulk of dense CO_2. Hydrate formation has been found to be thermodynamically feasible but still very questionable given its mass transport limitations compared to other possible routes for hydrate formation under same conditions. The inclusion of impurities like nitrogen, argon and methane will not change these results significantly. The concentration of hydrogen sulfide in low (ppm range) would be enough to enhance the thermodynamic stability of possible forming hydrate. Nevertheless, it is the mass transport limitations that remain a major uncertainty and provide a likely obstacle in this hydrate formation route. Given the water mole fraction will likely amount to 10^{-3} or less, it is quite questionable whether this route will be significant compared to other options for hydrate formation.

Routes 6 and 8: Hydrate formation involving condensed water and hydrate formers from the carbon dioxide stream

Using equation (6) for water in the condensed liquid phase and residual thermodynamics (equation (4)) for water dissolved in CO_2 fluid, one will obtain the following relationship between the mole fraction of water dissolved in CO_2, $y_{w,CO2}$,and that of water dropping out as liquid in aqueous phase, $x_{w,H2O}$:

$$x_{w,H2O}\gamma_{w,H2O}(T,P,\vec{x})\phi_w^{puregas}(T,P_w^{sat})P_w^{sat}(T)e^{\int_{P_w^{sat}}^{P}\frac{\overline{v}_{w,H2O}}{RT}dP} = y_{w,CO2}\phi_{w,CO2}(T,P,\vec{y})P \quad (13)$$

In case of hydrogen sulfide dissolved in carbon dioxide, we have to distinguish between carbon dioxide in a liquid state or as gas. For the latter case the appropriate fugacity relationship will be

$$x_{i,H2O}\gamma^{\infty}_{i,H2O}f^{\infty}_{i,H2O}(T,P_0)e^{\int_{P_0}^{P}\frac{v^{\infty}_{i,H2O}(T,P,\vec{x})}{RT}dP} = y_{i,CO2}\phi_{i,CO2}(T,P,\vec{y})P \quad (14)$$

where the left hand side will apply to the liquid water phase and i would be either CO_2 or H_2S when approximately neglecting drop-out of nitrogen, argon and methane. The left hand side will thus reduce to a Henry's law type of expression and right hand side can be evaluated using an adequate equation of state that can handle H_2S and CO_2 with proper accuracy. Equation (13) for water and equation (14) for CO_2 and H_2S respectively can then be rearranged into ratios of mole-fraction gas versus mole-fraction liquid of the same component (gas/liquid K-values) and used together with mass conservation to find amount of liquid condensed at local pressure and temperature as well as composition of the condensed phase. In chemical engineering this is normally denoted as a an isothermal flash-calculation. For the region where CO_2 is liquid of dense supercritical equation (14) has to be replaced by:

$$x_i\gamma^{\infty}_{i,H2O}f^{\infty}_{i,H2O}(T,P_0)e^{\int_{P_0}^{P}\frac{v^{\infty}_{i,H2O}(T,P,\vec{x})}{RT}dP} = y_i\gamma^{\infty}_{i,CO2}f^{\infty}_{i,CO2}(T,P_0)e^{\int_{P_0}^{P}\frac{v^{\infty}_{i,CO2}(T,P,\vec{x})}{RT}dP} \quad (15)$$

While carbon dioxide in the liquid or dense fluid region will be most conveniently handled by equation (14), an excess scheme (equation (5) and (6)) is possible as well. In summary, equation (13) applies to water over all the relevant conditions (sub critical water), and equation (14) applies to carbon dioxide. In case of hydrogen sulfide, equation (14) applies to the sub-critical CO_2 phase and equation (15), the super-critical CO_2 phase. Rearranging into gas/liquid equilibrium constants:

$$K_i^{CO2/H2O}(T,P,\vec{y},\vec{x}) = \frac{y_{i,CO2}}{x_{i,H2O}} \quad (16)$$

we arrive at:

$$K_w^{CO2/H2O}(T,P,\vec{y},\vec{x}) = \frac{\gamma_{w,H2O}(T,P,\vec{x})\phi_w^{puregas}(T,P_w^{sat})P_w^{sat}(T)e^{\int_{P_w^{sat}}^{P}\frac{\bar{v}_{w,H2O}}{RT}dP}}{\phi_{w,CO2}(T,P,\vec{y})P} \quad (17)$$

$$K_i^{CO2/H2O}(T,P,\vec{y},\vec{x}) = \frac{\gamma^{\infty}_{i,H2O}f^{\infty}_{i,H2O}(T,P_0)e^{\int_{P_0}^{P}\frac{v^{\infty}_{i,H2O}(T,P,\vec{x})}{RT}dP}}{\phi_{i,CO2}(T,P,\vec{y})P} \quad (18)$$

$$K_i^{CO2/H2O}(T,P,\vec{y},\vec{x}) = \frac{\gamma^{\infty}_{i,H2O}(T,P,\vec{x})f^{\infty}_{i,H2O}(T,P_0)}{\gamma^{\infty}_{i,CO2}(T,P,\vec{y})f^{\infty}_{i,CO2}(T,P_0)}e^{\int_{P_0}^{P}\frac{\left[v^{\infty}_{i,H2O}(T,P,\vec{x})-v^{\infty}_{i,CO2}(T,P,\vec{y})\right]}{RT}dP} \quad (19)$$

This is an equilibrium calculation for the specific evaluation of impact of water liquid drop-out and subsequent risk of hydrate formation. As such the chemical potential of all components in dropped out liquid and the CO_2 phase are identical and hydrate formation conditions will as such be the same. This is more or less the typical present standard for hydrate risk evaluation in industry. One way to proceed is to estimate the amount of liquid drop-out and composition by solving the mass conservation under equilibrium conditions for given temperature and pressure, resulting in:

$$\sum_{i=1}^{n} \frac{(K_i^{CO2/H2O} - 1)z_i}{(1-\alpha)K_i^{CO2/H2O} + \alpha} = 0 \quad (20)$$

Equation (20) is known as the flash equation, detailed explanations of its application are readily available in chemical engineering textbooks dealing with technology. z_i denotes the initial mole-fractions in the CO_2 mixture, and α is the liquid (water) phase fraction of the initial CO_2 phase. Assuming that the trace amounts of nitrogen, argon and methane drop out will be negligible, the number components, *n*, would still be equal to 6, although only three of them (water, hydrogen sulfide, and carbon dioxide) will require a detailed estimation of their gas/liquid K-values, while those components assumed to remain entirely in the gas phase can be given sufficiently large values of K. The composition of the aqueous phase will be given by:

$$x_i = \frac{z_i}{(1-\alpha)K_i^{CO2/H2O} + \alpha} \quad (21)$$

and the composition of the remaining gas phase:

$$y_i = \frac{(K_i^{CO2/H2O} - 1)z_i}{(1-\alpha)K_i^{CO2/H2O} + \alpha} \quad (22)$$

Since P and T are always specified locally in a flow situation, the solution of equation (20) would provide the most rigorous estimation of the amount and the composition of liquid dropping out at the given T and P. These composition estimates can be used to evaluate the hydrate formation possibilities following routes 6 and 8 in table 1. This approach can also easily handle guest combinations, for example, H_2S from aqueous solution and CO_2 from fluid.

A slightly simpler option which might be easier to implement in current industrial codes would be to estimate the water content needed for water condensation at the given pressure and temperature. One can then assume that condensed water droplet will be saturated with H_2S and CO_2 (i.e. neglect nitrogen, argon and methane solubility in water). Then the same analysis as above can be conducted (options 6 and 8 and combinations).

Fundamental equilibrium thermodynamics of hydrate

Applying the statistical mechanical model for water in hydrate [1]:

$$\mu_{w,H} = \mu_{w,H}^{O} - \sum_{k=1,2} RTv_k \ln\left(1 + \sum_i h_{ik}\right) \quad (23)$$

where H denotes hydrate phase, superscript 0 stands for empty hydrate, v_k is the fraction of cavity of type k per water. For structure I hydrate this is 1/23 for small cavities (20 water molecules) and 3/23 for large cavities (24 water molecules). h_{ik} is the canonical partition function for a cavity of type k containing a molecule of type i and is given by:

$$h_{ik} = e^{\beta\left(\mu_i^H - \Delta g_{ik}^{inc}\right)} \quad (24)$$

where β is the inverse of the gas constant times temperature and Δg_{jk}^{inc} reflects the impact on hydrate water from the inclusion of the "guest" molecule i in the cavity [1]. At equilibrium the chemical potential μ_i^H has to be equal to the corresponding chemical potential in the phase where molecule i was extracted from. The hydrate content of all gas components can be estimated by applying equation (4) to calculate their chemical potential when dissolved in the carbon dioxide phase. The chemical potential of liquid water will be somewhat affected by the presence of hydrogen sulfide and carbon dioxide, with the concentration of hydrogen sulfide in the different phases significantly affecting the results. Solving equation (20) for the temperature and pressure of interest will yield the maximum drop-out of the aqueous phase, while the solution for hydrate formation will only have one

degree of freedom. This means that the hydrate forming pressure has to be solved in an iterative loop together with equations (20) to (22) to ensure that gas compositions and chemical potentials, as well as liquid water compositions and chemical potential for water are appropriate for the actual hydrate forming pressure that satisfies (25).

$$\mu_w^{O,H} - \sum_{k=1,2} RTv_k \ln\left(1+\sum_i h_{ik}\right) = \mu_{i,H2O}^{purewater}(T,P) + RT\ln\left[x_{i,H2O}\gamma_{i,H2O}(T,P,\vec{x})\right] \quad (25)$$

Note that chemical potentials of the empty hydrate structure estimated basing on Kvamme & Tanaka [1] have been verified to have predictive capabilities, which makes any empirical formulations for these unnecessary. If the estimated hydrate formation pressure is lower than the local one, the hydrate will form following this particular route.

Besides being unable to reach equilibrium, as discussed earlier, the system under consideration will be distinguished by the drastic disparity in hydrate forming abilities exhibited by impurities dissolved in carbon dioxide. H_2S is known for being an extremely aggressive hydrate former, while nitrogen is located at the opposite end of the scale. So a more realistic evaluation of this route to hydrate formation will have to start from a dew-point approach for water drop-out, with H_2S and CO_2 being considered as condensing components together with water, similar to the approximation above. If the dew-point pressure is lower than the local pressure, water will drop out as a liquid phase. In this case one can assume that free water will be available and the lowest free energy hydrate will form. In contrast to the "classical" calculations, this approach would not consider the usual hydrate formation from the "bulk" gas but rather search for hydrate with the absolute lowest free energy that could nucleate from the available carbon dioxide mixture. In other words, one would aim to minimize the following equation in terms of hydrate formation pressure while taking into account the fact our system will be unable to reach equilibrium.

$$G^H = \sum_i x_i^H \mu_i^H \quad (26)$$

The non-equilibrium description of hydrate due to Kvamme et. al [2] can be applied for this purpose to follow the gradients in free energies until the carbon dioxide phase has been mostly depleted in the most aggressive hydrate former, hydrogen sulfide. The analysis of equation (26) will also require the hydrate composition; it can be found by applying from the statistical thermodynamic theory to the adsorption model for hydrate (equation (23)) and will be given by

$$\theta_{ik} = \frac{x_{ik}^H}{v_k\left(1-x_T\right)} = \frac{h_{ik}}{1+\sum_i h_{ik}} \quad (27)$$

where θ_{ik} is the filling fraction of component in cavity type k, x_{ik}^H is the mole fraction of component i in cavity type k, x_T is the total mole fraction of all guests in the hydrate, and v_k is, as defined above, the fraction of cavities per water of type k.

The free energy of inclusion in equation (24) can be estimated according to Kvamme & Tanaka [1]. At this stage no attempts have been made to tune the model empirically to fit experimental data available in open literature. Thermodynamic consistency has been a high priority throughout this work. Since the molecular interaction model for CO_2 in this work is different from that of Kvamme & Tanaka [1] new free energy of inclusion functions parameters for this model, as well as for the H_2S model, have been estimated and listed in table 2 below (complementary to table 5 of Kvamme & Tanaka [1]). As an approximation we do not consider filling of small cavities although there are evidence that CO_2 can enter small cavity. But the stabilization impact is questionable and it is quite uncertain whether CO_2 filling in small cavities would happen under dynamic conditions.

Table 2. Calculated free energies of quest inclusion in the large cavity of structure I fitted to the function $\Delta g^{inclusion} = \sum_{i=0}^{5} k_0 \left[\frac{a}{T}\right]^i$, where a is set to 1.0 for H_2S and equal to the critical temperature in case of CO_2

k_i	CO_2	H_2S
k_0	38.235921376606330	-119.3497
k_1	5.186549207819319	35256.6857
k_2	1.503361418932734	-6458174.13
k_3	-79.721232458662830	$4.782747311726352 \cdot 10^8$
k_4	-3.644403135129193	0
k_5	13.895740347159070	0

Figure 1 compares the estimated hydrate equilibrium curve for the CO_2 hydrate with the available experimental data from Ng & Robinson [7] and Larson [8]. The Soave-Redlich-Kwong (SRK) equation [9] was used to evaluate the deviations from ideal gas behavior via the fugacity coefficient. The ideal gas contribution was estimated using the CO_2 model due to Panhuis et.al. [10], which was the one used for molecular dynamics studies involving carbon dioxide dissolved in water. Given that carbon dioxide density was also found via a spherical van der Waal-type equation of state (SRK), the equilibrium curve will be less smooth than hydrate curves derived for the hydrate former phases. The significant deviations in the lower pressure region can be traced back to the combination of models described above. Since these temperatures and pressures lie outside the most relevant and critical conditions, the model systems were deemed satisfactory enough for the purposes of further analysis. A similar approach was used to analyze the H_2S hydrate formation. The SRK equation of state used to calculate density and fugacity coefficients, while the model due to Kristóf & Liszi [11] employed to estimate the ideal gas chemical potential. The resulting hydrate equilibrium curve for H_2S hydrate is plotted and compared to experimental data from Bond & Russel [12] in figure 2.

A critical question that has to be answered here is how the formation of H2S-dominated hydrate will compete with formation of CO2-dominated hydrate assisted by presence of H2S. Figure 3 presents the estimated chemical potential of water as stabilized by either a CO2 -- H2S mixture or H2S alone for H2S mole fraction of 0.001, 0.003 and 0.025 at pressures 100 and 200 bar.
These comparisons indicate that at these concentrations, H_2S will only be able to assist carbon dioxide in stabilizing the CO_2-dominated hydrate rather than produce any competing H_2S hydrate. As such, the risk of hydrate formation from carbon dioxide phase with impurities and free water can be evaluated in terms mixture stabilization of hydrate.

Relative impacts of routes 7 through 10

The surface reformation (denoted as route 7 in table 1) will play a crucial role in a number of hydrate phase transition phenomena ranging from hydrate nucleation to stable growth to massive growth (induction). Hydrate forming on the interface between water and a hydrate former will be significantly non-uniform and will quickly create a film layer. This layer will severely inhibit the rate of mass transport of hydrate formers from one phase into another that will lead to consumption of particles with higher free energy to favour the further growth of hydrate regions with lower free energy. This mechanism is one of several factors that will delay the massive hydrate growth in zones where hydrodynamic shear forces are too weak to break up the hydrate layers. This route has been investigated by different groups experimentally as well as theoretically. Some examples are given elsewhere [3-5].
The analysis of homogeneous hydrate formation from aqueous solution in Kvamme [3, 4] indicated that the stability region of carbon dioxide hydrate will be substantially shifted when water-soluble hydrogen sulfide is present but remain essentially unaffected in case of argon, nitrogen and methane due to their extremely low solubility into water. The adsorption of water on hematite investigated in [6] clearly showed that water may derive substantial thermodynamic benefits from adsorbing as a layer on the hematite surface as compared to condensing out as liquid water. This finding makes routes 9 and 10 into alternatives which are likely to out-compete hydrate formation via routes 6 and 8. Our adsorption study [6] has also shown that the two-dimensional adsorbed water structure on appeared to be a compromise between water – water hydrogen bonds and electrostatic interactions between water and ions belonging to hematite crystalline structure. This led to creation of dynamic "pockets" which might leave room for adsorption of smaller guest molecules like argon, nitrogen and methane but which will not be particularly beneficial for larger carbon dioxide molecules.

The implications of non-equilibrium thermodynamics

The non-equilibrium aspects of hydrate phase transitions discussed above impose substantial experimental challenges related to experiments in the hydrate stability regions of temperatures and pressures since the carbon dioxide solubility is dominated by the impact of the hydrate phase, which is the phase of chemical potential for water in the hydrate stability region. As a consequence,

the solubility of carbon dioxide is lower than what could be expected if the system did not contain hydrate. This can be verified by limited range extrapolations of Henry's law (rigorous version) into the hydrate region. The difference in concentration between the hydrate controlled maximum carbon dioxide in water and the dissolved carbon dioxide in water is the amount of hydrate that can be produced from carbon dioxide dissolved in water [2, 3]. And the impact of solid surfaces adds additional challenges to interpretations of experiments. We have not so far found any experiments that in some way try to quantify the impact of solid water-wetting surfaces on carbon dioxide solubility in hydrate controlled regions. In view of this many of the estimates here are without experimental data for comparison at this stage since even the most recent experiments on carbon dioxide solubility in hydrate forming regions may not have clear interpretations in view of the discussion above. Hydrate nucleation and growth in non-equilibrium will be facilitated by heterogeneous nucleation (solid surfaces and hydrate former/water surface) and since chemical potentials of hydrate formers and water may differ from bulk phase properties of these the compositions and free energies of the hydrates formed will be different. Different experimental facilities with varying materials and set-ups that give rice to variations in the progresses of hydrate formation impose uncertainties.

The challenge of non-equilibrium thermodynamics and hydrate phase transitions that are competing can be handled on different levels and some strategies are discussed elsewhere (see [2, 6] and references therein) and supplemented with corresponding equations for hydrate sub and super saturation in this paper. At the lack of some rigor a simplified discrete evaluation scheme is illustrated here. This scheme can be easily implemented as extensions of industrial hydrate risk evaluation codes in a possible events scheme, and corresponding levels of acceptable carbon dioxide content. Rigorous schemes [2, 6] do require consistent reference values for thermodynamics of all phases interacting with the hydrate.

Numeric simulations of fluid bulk systems

We have applied the MDynaMix program package [13] to perform NVT and NPT molecular dynamics simulations that provided data needed to estimate chemical potential and free energy. The force fields included TIP4P model for water [14], Kristóf and Liszi model for H_2S [11], and the EPM2 [15] and the Panhuis et al [10] models for CO_2.

NVT simulations require the knowledge of pressure-dependent densities of the bulk fluid phases (either predominantly CO_2 or H_2O). The density of CO_2 at different pressures and temperatures has been extensively tabulated by Span and Wagner [16]. Densities used as input for our simulations were obtained using the online calculators for water and CO_2 by Wischnewski [17, 18]. The calculator-provided values for two temperatures unavailable in [16] were found consistent with the tabulated results.

CO_2 dissolved in water

We have used the techniques of molecular simulation to estimate the chemical potential of water with dissolved carbon dioxide for a range of temperatures, pressures and carbon dioxide concentrations relevant for CO2 transport and hydrate formation. The chemical potential was evaluated following thermodynamic integration along a polynomial path due to Mezei [19]. A set of simulations was run at 278.15 K and overall bulk density of 0.9997 g/cm^3. The partial molar volume of water in water is equal to 18 cm^3/mol, while the partial molar volume of CO_2 is 32 cm^3/mol and 33 cm^3/mol at 0°C and 20°C respectively. At these temperatures, setting the partial molar volume of CO_2 to be 32.5 cm^3/mol will be sufficiently accurate [20]. The ideal gas chemical potential at 278.15 K was estimated based on the same carbon dioxide model as employed by the MD simulations; it was to be equal to -26.81 kJ/mol for H_2O and -41.12 kJ/mol for CO_2. Though some pressure-dependent variations will always be present, their effect on the chemical potential of CO_2 will be very small, and the contribution to the total chemical potential can safely be neglected.

The total gas chemical potential ranged from -50.98 kJ/mol for pure water to -50.61 kJ/mol in case of CO_2 dissolved in H_2O at 5°C, 1 atm and a relatively high mole fraction of 0.047. We have also conducted simulations for pressures of 100 to 200 bar with CO_2 concentration ranging up to 0.005 and found that the effect of CO_2 concentration and pressure on the chemical potential to be hard to discern. On the other hand, temperature had a significant impact, at 1°C the chemical potential is -50.76±0.02 kJ/mol, at 5°C the range is 50.98±0.01 kJ/mol, and at 10°C the range is -51.26±0.01 kJ/mol.

H_2S dissolved in water

A number of simulations involving with H_2S dissolved in water were conducted using the thermodynamic temperature integration approach rather than Mezei's technique. A range of NPT simulations have been run at temperatures ranging between 274.15 K and 3000 K. The resulting potential energy curve $E_P = E_P(T^{-1})$ has been integrated as the function of inverse temperature, with the potential energy set exactly to 0 at T^{-1}.

The residual chemical potential per Kelvin Y at a given temperature T_1 will then be given by:

$$\left(\frac{\mu_{H_2S,H_2O}}{RT}\right)_{T,P}-\left(\frac{\mu_{H_2S,H_2O}}{RT}\right)_{T\to\infty,P}=\int_0^T\frac{E_{P,H_2S,H_2O}}{R}d\left(\frac{1}{T}\right)+\left(\frac{PV}{RT}\right)_{T,P}-\left(\frac{PV}{RT}\right)_{T-\infty,P}$$

$$=\int_0^T\frac{E_{P,H_2S,H_2O}}{R}d\left(\frac{1}{T}\right)+\left(\frac{P\bar{V}^{\infty}_{H_2S,H_2O}}{RT}-1\right) \quad (28)$$

where the first term on the left hand side is the total chemical potential and the second term will correspond to the ideal gas since the influence of any interactions will be increasingly damped as the temperature approaches infinity. The last term on right hand side converts residual energy into residual enthalpy. $\bar{V}^{\infty}_{H_2S,H_2O}$ is the partial molar volume of H_2S in aqueous solution.
The simulations were conducted using 512 water molecules and between 1 and 4 H_2S molecules. Increasing the number of H_2S molecules from 1 to 4 changed the total chemical potential from -54.16 kJ/mol to -54.12 kJ/mol, and it increased the volume of the system from 15361 Å³ to 15520 Å³.
Since H_2S molecules are quite similar to water molecules structurally, this set of simulations allows us to calculate the partial molar volume of H_2S in water in a straightforward manner by simply observing the volume change caused by the additional H_2S molecules. We calculated a partial molar volume of 32.2 cm^3/mol, a value that agrees well with both theoretical value of 30.8 cm^3/mol and experimental value of 34.8 cm^3/mol given in Lepori and Gianni [21].

Another set of simulations were also conducted for H_2S concentrations between 0 and 0.003 and pressures spanning the range between 100 and 200 bar with temperatures varying from 1°C to 10°C. These pressure and temperature conditions were also tested for a case of a high 5mol% concentration of H_2S. Though pressure variation and small changes in H_2S concentration between 0 and 0.003 did have a minor impact on the chemical potential, the effect remained inside the error bars. At 1°C the chemical potential is -50.76 ± 0.01 kJ/mol, at 5°C it is -50.98 ± 0.01 kJ/mol, and at 10°C it is -51.25±0.02 kJ/mol. Increasing the H_2S concentration up to 0.05 has resulted in lowering the total chemical potential by about 0.65 kJ/mol.

H_2S dissolved in carbon dioxide

MOLAR VOLUME OF H2S DISSOLVED IN CO2

Unlike the H2S in water scenario, H2S molecules have a very dissimilar structure to the CO2 molecules, and the presence of H2S molecules can therefore significantly affect the packing of the CO2 fluid. To estimate the partial molar volume, we have applied the first shell approach to the radial distribution function (RDF), $g(r)$, characteristic for H2S dissolved in the bulk of CO2 . The molar volume, vm, will then be given by the following equation

$$v_m = 4\pi \int_0^{r(g_{\max})} g(r)r^2dr \quad (30)$$

where *g(r)* denotes the location of the RDF's first peak. Unlike the case of monoatomic systems, a care must be taken when applying equation (30), since the actual *g(r)* involved in the integration must correspond to the site-site pair that determines the volume-filling characteristics. Alternatively, time-consuming molecular correlations functions have to be sampled or reconstructed approximately through the superposition method.

We used a simulation involving 4 H_2S molecules dissolved in 996 CO_2 molecules, with its sulfur versus oxygen radial distribution function plotted in figure 4. In this case, the first peak was located at about 3.55Å, and the numeric evaluation of the integral yielded the molar volume of 31.4 $Å^3$/molecule, or about 18.9 cm^3 per mole, which corresponds to the density of 1.8 kg/dm^3.

IDEAL GAS POTENTIALS

Corresponding Ideal gas chemical potentials are given by straightforward application of classical mechanics using the average moments of inertia for the rotational part.

In case of carbon dioxide, the density is known a priori, since as it is bulk fluid. The density of hydrogen sulfide has been earlier being estimated as equal to 1.8 kg/dm^3.

Under the extensive formulation, the extensive Gibbs free energy in kJ will be given by

$$\underline{G} = N_{H_2S,CO_2}\mu_{CO_2,CO_2} + N_{H_2S,CO_2}\mu_{H_2S,CO_2}$$
$$\approx \left[\text{-3.91596-4.72069x}_{H_2S,CO_2} + 674.201\text{x}^2_{H_2S,CO_2}\right](N_{CO_2} + N_{H_2S})$$
$$= \left[\text{-3.91596}(N_{H_2S,CO_2} + N_{H_2S,CO_2})\text{-4.72069}N_{H_2S,CO_2} + 674.201\frac{N^2_{H_2S,CO_2}}{(N_{H_2S,CO_2} + N_{H_2S,CO_2})}\right] \quad (31)$$

The residual chemical potential of pure CO_2 will be equal to -3.916 kJ/mole in the example used here.

Furthermore,

$$\lim_{N_{H_2S}\to 0}\left|\frac{\partial \underline{G}}{\partial N_{H_2S}}\right| = \mu^{R,\infty}_{H_2S,CO_2} = -8{,}63665 \text{ kJ/mole} \quad (32)$$

The gradient in question can be found from a second order fit to simulation data for H_2S dissolved in CO_2 at temperatures between 274.15 K and 283.15 K, and pressures ranging from 100 bar to 200 bar. This will establish the two necessary reference states; symmetric excess thermodynamics for CO_2 and non-symmetric excess thermodynamics for H_2S dissolved in CO_2. Formulating the molar free energy as function of mole-fractions, we arrive at:

$$G(T,P,\vec{x}_{CO2}) = x_{CO_2}\mu^{pure}_{CO_2,CO_2}(T,P) + RT\ln\left[x_{CO_2,CO_2}\gamma_{CO_2,CO_2}(T,P,\vec{x}_{CO_2})\right]$$
$$+(1-x_{CO_2,CO_2})\mu^{\infty}_{H_2S,CO_2}(T,P) + RT\ln\left[(1-x_{CO_2,CO_2})\gamma^{\infty}_{H_2S,CO_2}(T,P,\vec{x}_{CO_2})\right]$$
$$\approx x_{CO_2}\mu^{pure}_{CO_2,CO_2}(T,P) + RT\ln\left[x_{CO_2,CO_2}\right]$$
$$+(1-x_{CO_2,CO_2})\mu^{\infty}_{H_2S,CO_2}(T,P) + RT\ln\left[(1-x_{CO_2,CO_2})\gamma^{\infty}_{H_2S,CO_2}(T,P,\vec{x}_{CO_2})\right] \quad (33)$$

for which the approximation of activity coefficient equal to 1 for CO_2 is justified by the small concentration of H_2S in CO_2.

Defining G^M as:

$$G^M(T,P,\vec{x}_{CO_2}) = G(T,P,\vec{x}_{CO_2}) - x_{CO_2}\mu^{pure}_{CO_2,CO_2}(T,P) - (1-x_{CO_2,CO_2})\mu^{\infty}_{H_2S,CO_2}(T,P)$$
$$-RT\ln x_{CO_2,CO_2} - RT\ln\left[1-x_{CO_2,CO_2}\right] = RT\ln\left[\gamma^{\infty}_{H_2S,CO_2}(T,P,\vec{x}_{CO_2})\right] \quad (34)$$

Both activity coefficients based on infinite dilution as reference have been estimated together with infinite dilution properties, they can be made available on request. The solubility of water into CO2 is small and the amounts of H2S is very small (in practice, concentrations of H2S rarely exceed 600 ppm). For pure CO2 as the solvent, the individual parameters may, as a good approximation, therefore also be used for carbon dioxide containing both water and hydrogen sulfide. The impact of the other impurities (argon, methane and nitrogen) when carbon dioxide is still liquid may be treated by perturbation expansion from pure carbon dioxide solvent. Carbon dioxide gas range is not critical in this project since most of the region of transport is above 50 bars. But in that case the challenge is reliable estimates for water fugacity coefficients. Given that all the other components can be treated by an adequate choice of equation of state then Gibbs-Duhem might be a choice for calculation of water fugacity coefficient [2]. Also note that the fitting for activity coefficients are for small enough concentrations of H2S and CO2 in water for

these to be considered as approximately independent. This will of course not be valid for concentration ranging upward to solubility limits but this would be more convenient to fit into specific multi components activity coefficient models which are in use by the different users of the results presented here. For these high concentrations, a coupled reaction/phase transition model should be used.

H_2O dissolved in carbon dioxide

Water has a low solubility in any gas phase since water molecules have a strong tendency to cluster together due to hydrogen bonding. The solubility is somewhat higher in CO_2 than in air, but still much lower than that of CO_2 in water. The mutual solubility of these fluids has been subject to extensive studies, and a table of solubility for various pressure and temperature conditions and be found in the Appendix of Spycher, Pruess and Ennis-King [22]. Generally, the solubility of water in CO_2 at typical pipeline temperatures is on the order of 2000 ppmv.
To deal with the low solubility a fairly large system with only a few water molecules had to be applied. For the systems with up to 4 H_2O molecules, we used a total of 2000 molecules. The systems with only one or two H_2O molecules had a total of 1000 molecules. Calculations of the excess free energy were calculated using Mezei's method. The density of carbon dioxide was 0.8970 g/cm^3. In these conditions, the ideal gas chemical potential of CO_2 is -46.7627 kJ/mol. The total chemical potentials ranged from -45.883 kJ/mol for pure water to -45.899 kJ/mol for H_2O concentration of 0.002. Using the RDF between the CO_2 carbon and the H_2O oxygen, equation (30) yielded an estimate of the partial molar volume of 28.8 cm^3, which translates into the partial density of water in CO_2 of about 0.63 g/cm^3. This value yielded the ideal gas chemical potential of water equal to -27.9005 kJ/mol.

We have also performed a set of simulations similar to those for H_2S in water to ascertain the effect of pressure and temperature variations. The systems involved had 1000 molecules in total, with either one or two of them being water molecules. These simulations were conducted at temperatures 274.15, 278.15, and 283.15 K; and pressures 100, 150, and 200 bar. The chemical potentials ranged from -45.165 kJ/mol at 274.15 K and 200 bar to -46.688 kJ/mol at 283.15 K and 100 bar. Raising pressure from 100 to 200 bar has resulted in the total chemical potential increasing by about 0.05 kJ/mol ; it decreased by 1.45 kJ/mol as the temperature increased from 274.15 K to 283.15 K. The chemical potential also decreased slightly with increasing H_2O concentration, although this effect was somewhat obscured by noise.

Hydrate formation from liquid water with dissolved hydrate formers.

If the pressure and temperature fall inside the hydrate stability region, chemical potential of water in hydrate will be lower than that of liquid water. It does not necessarily mean that the hydrate as whole will be more stable than the surrounding fluid phase, since one must also take into consideration the chemical potential gradients of all hydrate constituents across the phase boundaries of co-existing phases. Thus hydrate will dissociate when in contact with pure water because the liquid phase will be under-saturated in the guest molecules. Furthermore, hydrate will sublimate towards gas or fluid if they are under-saturated with respect to water. Liquid water that condenses, and potentially accumulates, as aqueous phase in a pipeline will normally be saturated with respect to the carbon dioxide phase. When a hydrate forms, it will be supersaturated when it comes to hydrates that are lower in free energy, and will be able to grow from solution [3, 4, 23-25]. Even though the equilibrium cannot truly be possible, one can establish certain quasi-hydrate limits that will eventually also be useful in kinetic models.

With both temperature and pressure fixed locally the chemical potentials for hydrogen sulfide and carbon dioxide can be estimated from equation (9) with data for infinite dilution chemical potentials and activity coefficients derived from molecular modelling and experiments. These chemical potentials enter equation (23) in equilibrium calculation, in which it is assumed that hydrate chemical potentials is equal those in coexisting phase for the same components. On the other hand, with pressure and temperature both defined, the system is over-determined and equation (1) can be used to search for the lowest free energy hydrate possible, whether using non equilibrium thermodynamics [2] and free energy minimizing algorithms or less advanced approaches. After all, hydrogen sulfide is superior as a hydrate former compared to carbon dioxide so testing for optimum hydrogen sulfide filling from available mass of hydrogen sulfide in the liquid solution is sufficient. This is also the hydrate stability level (the degree of free energy of hydrate lower than liquid water phase) which must be considered in term of necessary amounts of hydrate inhibitors needed to change the sign of (1) due to lowered chemical potential of water.

Conclusions

The careful consideration of the Gibbs phase rule and the first and second laws of thermodynamics have shown that hydrate formation from water and other impurities will be unable to reach equilibrium. In this case, it is the free energy minimum that will govern both the local and the global progress of phase transitions. This will require the knowledge of consistent thermodynamic properties for all components across the phase boundaries. In this work, we have applied the combination of molecular dynamics simulations and classical thermodynamic relationships to estimate the chemical potentials for water, hydrogen sulfide and carbon

dioxide in all adsorbed phases, the aqueous solution, and the carbon dioxide phase. Other impurities like methane, nitrogen and argon have low water solubility and lack specific properties (polarity) that would facilitate their adsorption on the pipe walls in competition with water and more polar constituents like hydrogen sulfide and carbon dioxide. As such, these components will only be of relative importance as hydrate formers from the free liquid water phase and the carbon dioxide phase. The most likely sequence of events leading to hydrate formation, in terms of thermodynamics, will involve water dropping out primarily due to adsorption onto the rusty pipeline walls. The hydrate will start forming from the accumulated water film. In a possible revision of best practice for hydrate prevention it is therefore recommended to reduce water content in the carbon dioxide phase to a concentration less than the concentration that would lead to adsorption drop-out. The calculation procedure for this will be similar to calculating water dew-point but now with chemical potentials for adsorbed state of the relevant surface, which in this work was limited to Hematite. This can be extended to a similar analysis for other possible surfaces like for instance iron carbonates.

The primary source of carbon dioxide for this hydrate growth will be provided by the carbon dioxide being transported. The hydrogen sulfide impurities that will aid hydrate formation from the carbon dioxide may come from hydrogen sulfide dissolved in both water and carbon dioxide phases as well as hydrogen sulfide adsorbed on the walls. The presence of hydrogen sulfide can have drastic consequences for hydrate formation in case of its higher concentrations in carbon dioxide (> 0.1 mol %), since the high solubility of hydrogen sulfide in water will may facilitate formation and growth of a separate hydrogen sulfide phase from adsorbed and dissolved hydrogen sulfide. This simultaneous hydrate formation from dissolved and adsorbed hydrate formers, as well as hydrate growth on water/carbon dioxide interface, is likely to be very rapid since the hydrate growth rate will no longer be necessarily limited by mass transport across the hydrate film. The combination of ongoing mass transport, heat transfer, and phase transitions may also lead to dynamic hydrate dissociation and reformation. In this work, we have fully outlined a theoretical approach capable of evaluating the competing phase transitions under constraints of both mass and heat transport. Results presented here will also benefit simpler kinetic theories by strengthening their theoretical basis. In view of insights gained in this work, it would also be instructive to re-evaluate the mechanisms that govern kinetic hydrate inhibition.

Acknowledgments

We acknowledge the grant and support from Research Council of Norway through the following projects: SSC-Ramore, “Subsurface storage of CO2 - Risk assessment, monitoring and remediation”, Research Council of Norway, project number: 178008/I30, FME-SUCCESS, Research Council of Norway, project number: 804831, PETROMAKS, “CO2 injection for extra production”, Research Council of Norway, project number: 801445. Funding from Research Council of Norway, TOTAL and Gassco through the project “CO2/H2O+” is highly appreciated

Notes and references

[a] Universitetet i Bergen, Institutt for Fysikk og Teknologi, Allégaten 55, N-5007 Bergen, Norge. Fax: +47 55589440; Tel: +47 55583310; E-mail: bjorn.kvamme@ift.uib.no.

1 Citations here in the format A. Name, B. Name and C. Name, *Journal Title*, 2000, **35**, 3523; A. Name, B. Name and C. Name, *Journal Title*, 2000, 35, 3523. B. Kvamme, and H. Tanaka, “Thermodynamic Stability of Hydrates for Ethane, Ethylene, and Carbon Dioxide”, J. Phys.Chem., 1995, 99, 7114-7119

2 B. Kvamme , T. Kuznetsova , P.-H. Kivelæ and J. Bauman, “Can hydrate form in carbon dioxide from dissolved water?”, Phys. Chem. Chem. Phys., 2013, Advance Article DOI: 10.1039/C2CP43061D

3 B. Kvamme, “Kinetics of Hydrate Formation from Nucleation Theory”, Int. J. Offshore Polar Eng., 2002, 12(4), 256-263

4 B. Kvamme, “Droplets of Dry Ice and Cold Liquid CO2 for Self-Transport of CO2 to Large Depths”, Int. J. Offshore Polar Eng., 2003, 13(2), 139-146

5 B. Kvamme, A. Graue, E. Aspenes, T. Kuznetsova, L. Gránásy, G. Tóth, T. Pusztai, and G. Tegze, “Kinetics of solid hydrate formation by carbon dioxide: Phase field theory of hydrate nucleation and magnetic resonance imaging” Phys. Chem. Chem. Phys., 2004, 6, 2327-2334

6 B. Kvamme , T. Kuznetsova and P.-H. Kivelæ, “Adsorption of water and carbon dioxide on hematite and consequences for possible hydrate formation” *Phys. Chem. Chem. Phys.,* 2012, **14**, 4410-4424

7 H.-J.Ng, and D.B. Robinson, D.B., Fluid Phase Equilibria, 21, 145, 1985

8 Larson, S.D., “Phase studies of the two-component carbon dioxide – water system, involving the carbon dioxide hydrate”, Univ. of Illinois, 1955

9 G. Soave, “Equilibrium constants from a modified Redlich-Kwong equation of state”, *Chem. Eng. Sci*,1971, **27**, 1197-1203

10 M. In Het Panhuis, C. H. Patterson, R. M. Lynden-Bell, “A molecular dynamics study of carbon dioxide in water: diffusion, structure and thermodynamics”, *Mol. Phys*, 1998, **94**, 963-972

11 T. Kristóf, J. Liszi, “Effective Intermolecular potential for Fluid Hydrogen Sulfide”, *J. Phys. Chem.,* 1997, **101**, 5480-5483

12 D. C. Bond, N. B. Russell, "Effect of Antifreeze Agents on the Formation of Hydrogen Sulfide Hydrate". *Pet. Trans. AIME*, 1949, **179**, 192.
13 J. P. M. Jämbeck, F. Mocci, A. P. Lyubartsev, A. Laaksonen, "Partial atomic charges and their impact on the free energy of solvation". *J. Comput. Chem.*, 2013, **34**, 187-197.
14 W. L. Jorgensen, J. Chandrasekhar, J. Madura, R. W. Impey, M. L. Klein, "Comparison of simple potential function for simulating liquid water", *J. Chem. Phys*., 1983, **79**, 926-935
15 J. G. Harris, K. H. Yung, "Carbon Dioxide's Liquid-Vapor Coexistence Curve And Critical Properties as Predicted by a Simple Molecular Model", *J. Phys. Chem*, 1995, **99**(31), 12021-12024
16 R. Span, W. Wagner. "A New Equation of State for Carbon Dioxide Covering the Fluid Region from the Triple-Point Temperature to 1100 K at Pressures up to 800 MPa", *J. Phys. Chem. Ref. Data*., 1996, **25**(6), 1509-1594
17 B. Wishnewski. "Calculation of thermodynamic properties of water", http://www.peacesoftware.de/einigewerte/wasser_dampf_e.html
18 B. Wishnewski. "Calculation of thermodynamic properties of carbon dioxide", http://www.peacesoftware.de/einigewerte/co2_e.html
19 M. Mezei. "Polynomial path for the calculation of liquid state free energies from computer simulations tested on liquid water", J. Comput. Chem., 1992, 13(5), 651-656
20 H. Teng, S. M. Masutani, C. M. Kinoshita, G. C. Nihous, "Solubility of CO2 in the ocean and its effect on CO2 dissolution", Energy Convers. Mgmt, 1996, 37(6-8), 1029-1038
21 L. Lepori, P. Gianni, "Partial Molar Volumes of Ionic and Nonionic Organic Solutes in Water: A Simple Additivity Scheme Based on the Intrinsic Volume Approach", J. Solution. Chem, 2000, 29(5):405-447
22 N. Spycher, K. Pruess, E. Ennis-King, "CO2-H2O mixtures in the geological sequestration of CO2. I. Assessment and calculation of mutual solubilities from 12 to 100°C abd up to 600 bar", Geochimica et Cosmochimica Acta, 2003, 67(16), 3015-3031
22 B. Kvamme, A. Graue, T. Kuznetsova, T. Buanes, G. Ersland, "Storage of CO2 in natural gas hydrate reservoirs and the effect of hydrate as an extra sealing in cold aquifers", Int. J. Greenh. Gas Con., 2007, 1/2, 236
23 A. Svandal, "Modeling hydrate phase transitions using mean-field approaches", PhD Thesis, University of Bergen, 2006
24 B. Kvamme, A. Svandal, T. Buanes, T. Kuznetsova, "Phase field approaches to the kinetic modeling of hydrate phase transitions," AAPG Memoir, 2009, 89, 758 – 769
26 J. T. Vassdal (2010). "Molekylærdynamiske studier av vannadsorpsjon på hematitt." Institutt for fysikk og teknologi. Master thesis, University of Bergen, June 2010.
27 A. P. Lyubartsev, A. Laaksonen. "MDynamix - A scalable portable parallel MD simulation package for arbitrary molecular mixtures." Comput. Phys. Commun. 2000, 128, 565-589.
28 M. Qasim, B. Kvamme, K. Baig, "Phase field theory modeling of CH_4/CO_2 gas hydrates in gravity fields," *International Journal of Geology*, 2011, **5**(2), 48-52.
29 B. Kvamme, K. Baig, M. Qasim, J. Bauman, "Thermodynamic Modeling of CH_4/CO_2 hydrate Phase Transition", *International Journal of Energy and Environment*, submitted 2012
30 T. Buanes, "Mean-field approaches applied to hydrate phase transition kinetics", PhD thesis, University of Bergen, Norway, 2008
31 G. Tegze, L. Gránásy, "Phase field simulation of liquid phase separation with fluid flow," *Mat. Sci. Eng. A,* 2005*,* **413 – 414**, 418 – 422
32 M. Conti, "Density change effects on crystal growth from the melt," *Phys. Rev. E*, 2001, **64**, 051601
33 M. Conti, M. Fermani, "Interface dynamics and solute trapping in alloy solidification with density change," *Phys. Rev. E*, 2003, **67**, 026117.
34 M. Conti, "Advection flow effects in the growth of a free dendrite," *Phys. Rev. E*, 2004, **69**, 022601
35 P.-H. Kivelä, K. Baig, M. Qasim, B. Kvamme, "Phase Field Theory Modeling of Methane Fluxes from Exposed Natural Gas Hydrate Reservoirs", *AIP Conf. Proc*, 2012, **1504**, 351-363
36 B. Kvamme, T. Kuznetsova, D. Uppstad, "Modeling excess surface energy in dry and wetted calcite systems", *J. Math. Chem*., 2009, **46**(3), 756 – 762
37 B. Kvamme, T. Kuznetsova, "Investigation into stability and interfacial properties of CO_2 hydrate - aqeuous fluid system", *Math. Comput. Model*., 2010, **51**, 156-159
38 B. Kvamme, T. Kuznetsova, K. Schmidt, "Molecular dynamics simulations and numerical modelling of interfacial tension in water-methane systems", *WSEAS TRANSACTIONS ON Biology And Biomedicine*, 2006, **3**(7), 517 – 523
39 B. Kvamme, A. Lund A, T. Hertzberg " The influence of gas-gas interactions on the Langmuir constants for some natural gas hydrates", *Fluid Phase Equilibria*, 1993, **90**, 15 – 44

Appendix: Non equilibrium thermodynamics for super and sub saturation of H2S and CO2

Phase field theory (PFT) for simulations of phase transition kinetics in non-equilibrium systems is basically a free energy minimization of free energy under the constraints of mass and heat transport [2, 20-22, 29-36]. As discussed in the main body of the paper H_2S and CO_2 will dominate the initial onset of hydrate and as such represents the key risk issues. After the H_2S have been consumed CO_2 with different fillings small cavities will follow in subsequent hydrate formations and the most dominant extra guest that can stabilize small cavity in structure I will follow successively. Hydrate of structure I formed a mixture of CO_2 and CH_4 , with methane occupying the small cavities has been outlined before [2]. When mixed together, H_2S and CO_2 will

essentially compete for the large cavities, with the thermodynamics of this process outlined below. For simplicity's sake, we will assume that H_2S and CO_2 fill the large cavities only (in competition based on average filling fractions due to differences in cavity partition functions). This means that it would only be necessary need to evaluate for a single-component occupation of the small cavities since it will suffice to evaluate the relative stabilities of different guest entering the small cavities. As long as thermodynamics is defined within the same framework for all of the phases to ensure consistent thermodynamics across different phase boundaries (*ie* absolute thermodynamics), the PFT will be able to analyse the competing phase transitions. Though the interface free energies between carbon-dioxide-dominated fluid and the aqueous phase cannot be exactly equated to the interfacial tension, data from our earlier studies on carbon dioxide/water interfacial tensions [37 – 38 and references therein] might be used for a start. Solid/fluid free energies is more complex but our simulations results for chemical potentials of different adsorbed molecules also provides a strengthened potential for succeeding also in calculation interfacial free energies of these complex interfaces, which are needed in PFT. Unlike molecular dynamics simulations PFT work on a continuous scale of mole-fraction so there are no limits in mole-fractions downwards. It is important in this context that the gradients in free energies with respect to mole-fractions are independent in these formulations, which are intended for use PFT or similar modelling in which conservation of mole fraction conservation are implicit.

The Gibbs free energy of the hydrate phase can be written written as a sum of chemical potentials for each hydrate component [3, 6, 7, 15].

$$G_H = \sum\nolimits_{r=c,m,s,w} x_r \mu_r^H \qquad \text{(A-1)}$$

where μ^H and x_r is chemical potential and mole fraction of component r respectively (c for CO_2, s for H_2S, m for CH_4, w for water). G_H is the free energy of hydrate. In the earlier work due to Svandal and Kvamme et.al. [24,25] a simple interpolation in mole-fractions was used between pure CH_4 hydrate and pure CO_2 hydrate, which was considered as sufficient to theoretically illustrate the exchange concept under phase field theory. This will of course not reproduce the absolute minimum in free energy for a mixed hydrate in which CH_4 occupies portions of the small cavities and increases stability over pure CO_2 hydrate. The expression for free energy gradients with respect to mole fraction, pressure and temperature is:

$$G_H^{EXP} = G^{EQ} + \sum_{r}^{r=c,s,m,w} \frac{\partial G_H}{\partial x_r} dx_r + \frac{\partial G_H}{\partial P} dP + \frac{\partial G_H}{\partial T} dT \qquad \text{(A-2)}$$

Here G_H^{EXP} is the free of hydrate away from equilibrium. G^{EQ} is the free energy value at equilibrium. The sum over r uses c for carbon dioxide, and s for hydrogen sulfide, m for methane, and w for water. We are now seeking gradients in all directions, independent of mole-fraction conservation (sum of mole-fraction are conserved inside PFT). So in terms of super-saturations in mole-fractions, these have to be evaluated as orthonormal gradient effects. In simple terms that means:

$$\left(\frac{\partial x_z}{\partial x_r}\right)\begin{cases} 0, z \neq r \\ 1, z = r \end{cases} \qquad \text{(A-3)}$$

Where z and r both represent any of the components of the hydrate: carbon dioxide, hydrogen sulfide, methane, and water. This is just means that the mole fractions are all independent. Using equation (A-2) we simply take the derivative with respect to one of the mole fractions (r=c,s,m,or w) and the mole fraction derivatives becomes zero due to equation (A-3) for mole fraction independence, resulting in:

$$\frac{\partial G_H}{\partial x_r} = x_c \frac{\partial \mu_c^H}{\partial x_r} + x_m \frac{\partial \mu_m^H}{\partial x_r} + x_s \frac{\partial \mu_s^H}{\partial x_r} + x_w \frac{\partial \mu_w^H}{\partial x_r} + \mu_r \frac{\partial x_r}{\partial x_r} \qquad \text{(A-4)}$$

It has been shown previously [2] that the chemical potential of a guest molecule can be approximated to a high degree of accuracy and in gradient terms:

$$\mu_k^H = A\ln\left(x_k\right) + B \quad , \quad \frac{\partial \mu_k^H}{\partial x_r} = \left\{0, r \neq k\right\} \tag{A-5}$$

Where k and r both represents any of the components of the hydrate (carbon dioxide, hydrogen sulfide, methane, and water). For the gradient due to a guest molecule, these simplifications lead to:

$$\frac{\partial G^H}{\partial x_k} = x_k \frac{\partial \mu_k^H}{\partial x_k} + \mu_k^H \tag{A-6}$$

The corresponding expression for water will include two more terms:

$$\frac{\partial G_H}{\partial x_w} = \sum_{r=m,w,c,s} x_r \frac{\partial \mu_r^H}{\partial x_w} + \mu_w^H \tag{A-7}$$

The chemical potential of a guest in the hydrate μ_k^H can be written as (Kvamme and Tanaka [1])

$$\mu_k^H = \Delta g_{kj}^{inc} + RT\ln\left(h_{kj}\right) \tag{A-8}$$

where Δg_{kj}^{inc} is the Gibbs free energy of inclusion of guest molecule k in cavity j, h_{kj} the cavity partition function of component k in cavity j, The universal gas constant is R and T is temperature. The derivative of equation (A-8) with respect to an arbitrary molecule r is:

$$\frac{\partial \mu_k^H}{\partial x_r^H} = \frac{\partial \Delta g_{kj}^{inc}}{\partial x_r^H} + \frac{\partial\left(RT\ln\left(h_{kj}\right)\right)}{\partial x_r^H} \tag{A-9}$$

The first term of equation (A-9), the stabilization energy is either evaluated as the langmuir constant or using harmonic oscillator approach [1]. In either case it is assumed to be approximately independent of temperature and pressure. Omitting the first term of (A-9) and approximating impacts of guest-guest interactions to be zero we arrive at:

$$\frac{\partial \mu_k^H}{\partial x_r^H} = \frac{RT}{h_{kj}} \frac{\partial h_{kj}}{\partial x_r^H} \tag{A-10}$$

The validity of omitting guest-guest interactions may be questionable for some systems [39] even though it is omitted in most hydrate equilibrium codes or empirically corrected for. Extensions for corrections to this can be implemented at a later stage.

The chemical potential of water will be expresses in the following way:

$$\mu_w^H(T,P,\vec{\theta}) = \mu_w^{0,H}(T,P_0) - \sum_j RT\nu_j \ln\left(1+\sum_k h_{kj}\right) \quad \text{(A-11)}$$

where $\mu_w^{0,H}$ is the chemical potential of water in an empty hydrate structure, The first sum is taken over both small and large cavities, the second one is over the components k in the cavity J. Here ν_j is the number of type-J cavities per water molecule. Hydrate structure I contains 3 large cavities and 1 small cavity per 23 water molecules, $\nu_l = 3/23$ and $\nu_s = 1/23$. The paper by Kvamme & Tanaka [3] provides the empty hydrate chemical potential as polynomials in inverse temperature, the Gibbs free energies of inclusion, and chemical potential of pure water, $\mu_w^{pure}(T)$. The derivative for the above equation with respect to an arbitrary molecule r results in:

$$\frac{\partial \mu_w^H}{\partial x_r} = -RT\sum_j \nu_j \left[\frac{\sum_k \frac{\partial h_{kj}}{\partial x_r}}{\left(1+\sum_k h_{kj}\right)}\right] \quad \text{(A-12)}$$

Equations (A-10) and (A-12) can be used to evaluate the derivative of the partition function basing on the following relationship between from the filling fraction and the partition function:

$$h_{kj} = \frac{\theta_{kj}}{1-\sum_i \theta_{ij}} \quad \text{(A-13)}$$

where θ_{kj} is the filling fraction of the components k in the cavity j. But it is easiest to recast everything in terms of mole fraction because of the basic assumption of mole fraction independence:

$$\theta_{kj} = \frac{x_{kj}}{\nu_j x_w} \quad \text{(A-14)}$$

Since we do not impose the constraint of mass conservation, the usual form of $1-x_T$ is not considered. This is substituted into equation (A-7) and we get:

$$h_{kj} = \frac{x_{kj}}{x_w \nu_j - \sum_i x_{ij}} \quad \text{(A-15)}$$

Taking the derivative with respect to an arbitrary component r and using equation (A-15) we obtain

$$\frac{\partial h_{kj}}{\partial x_r} = \frac{h_{kj}}{x_{kj}}\frac{\partial x_{kj}}{\partial x_r} - \frac{h_{kj}^2}{x_{kj}}\left(\nu_j \frac{\partial x_w}{\partial x_r} - \sum_i \frac{\partial x_{ij}}{\partial x_r}\right) \quad \text{(A-16)}$$

The first thing that must be dealt with the cavity mole fractions as a function of total mole fraction of a component:

$$x_k = \sum_j x_{kj} \quad \text{(A-17)}$$

Since the derivative of one mole fraction with respect to another is independent, the mole fraction in the cavity is also independent:

$$\left(\frac{\partial x_{kj}}{\partial x_r}\right)\begin{cases} 0, k \neq r \text{ or } r = w \\ 1, k = r \end{cases} \quad \text{(A-18)}$$

If $r = w$, then the derivative has to be zero because the guest mole fractions are independent of the mole fraction of water. Thus equation (A-16) can be simplified by using equation (A-17) and equation (A-18).

$$\frac{\partial h_{kj}}{\partial x_w} = -\frac{h_{kj}^2 \nu_j}{x_{kj}} \quad \text{(A-19)}$$

$$\frac{\partial h_{kj}}{\partial x_p} = \frac{h_{kj}}{x_{kj}}\frac{\partial x_{kj}}{\partial x_p} + \frac{h_{kj}^2}{x_{kj}}\frac{\partial x_{pj}}{\partial x_p} \quad \text{(A-20)}$$

where p is an arbitrary guest molecule, k is also an arbitrary guest molecule. These can be the same or different. If k and p are the same molecule, this gradient still exists and the "cross terms" are still able to be found even if there is independency in the mole fractions. dx_{kj} / dx_k is calculated by starting with the equation (A 18) which is the basic definition of the mole fraction of the cavities and how they relate to the total mole fraction of the component. The total methane mole fraction, x_m, is the sum of the mole fraction in the large cavities x_{ml}, and the mole fraction in the small cavities x_{ms} :

$$x_m = x_{ml} + x_{ms} \quad \text{(A-21)}$$

From discussion, it is assumed that there is a constant ratio between the partition functions and between different cavities of the same component. This is defined as A:

$$A \equiv \frac{h_{ml}}{h_{ms}} \quad \text{(A-22)}$$

The partition function can be written in terms of the filling fraction as shown in equation (A-13). Using equations (A-13), (A-12), (A-14) and assuming that the filling fraction of CO_2 and H_2S in small cavities are zero we get:

$$A = \frac{\frac{x_{ml}}{\nu_l x_w}}{\frac{x_{ms}}{\nu_s x_w}} \left(\frac{1 - \frac{x_{ms}}{\nu_s x_w}}{1 - \frac{x_{ml}}{\nu_l x_w} - \frac{x_{cl}}{\nu_l x_w} - \frac{x_{sl}}{\nu_l x_w}} \right) \tag{A-23}$$

This simplifies to:

$$x_{ml}\left[-\nu_s x_w\right] + x_{ms}\left[A\nu_l x_w - Ax_{cl} - Ax_{sl}\right] + x_{ms}x_{ml}\left[1-A\right] = 0 \tag{A-24}$$

Taking a derivative of above equation with respect to total methane mole fraction:

$$\left[x_{ms}\left(1-A\right) - \nu_s x_w\right]\frac{\partial x_{ml}}{\partial x_m}$$
$$+\left[A\nu_l x_w - Ax_{cl} - Ax_{sl} + x_{ml}\left(1-A\right)\right]\frac{\partial x_{ms}}{\partial x_m} = 0 \tag{A-25}$$

Substitutions were made to simplify the above equation and get it into a simpler form:

$$X = x_{ms}\left(1-A\right) - \nu_s x_w$$
$$Y = A\nu_l x_w - Ax_{cl} - Ax_{sl} + x_{ml}\left(1-A\right)$$

$$X\frac{\partial x_{ml}}{\partial x_m} + Y\frac{\partial x_{ms}}{\partial x_m} = 0 \tag{A-26}$$

Taking the derivative of equation (A-11) with respect to the total mole fraction of methane and simplification results in:

$$\frac{\partial x_{ml}}{\partial x_m} + \frac{\partial x_{ms}}{\partial x_m} = \frac{\partial x_m}{\partial x_m} = 1$$

$$\frac{\partial x_{ml}}{\partial x_m} = -\frac{Y}{X-Y}$$
$$\frac{\partial x_{ms}}{\partial x_m} = \frac{X}{X-Y} \tag{A-27}$$

Substituting the values of X and Y gives the final answer:

$$\frac{\partial x_{ml}}{\partial x_m} = -\frac{A\nu_l x_w - Ax_{cl} - Ax_{sl} + x_{ml}(1-A)}{x_{ms}(1-A) - \nu_s x_w - A\nu_l x_w - Ax_{cl} - Ax_{sl} + x_{ml}(1-A)}$$
$$\frac{\partial x_{ms}}{\partial x_m} = \frac{x_{ms}(1-A) - \nu_s x_w}{x_{ms}(1-A) - \nu_s x_w - A\nu_l x_w - Ax_{cl} - Ax_{sl} + x_{ml}(1-A)} \quad \text{(A-28)}$$

$\partial G_H / \partial P$ is calculated by taking derivative of equation (1) with respect to pressure.

$$\frac{\partial G_H}{\partial P} = x_c \frac{\partial \mu_c^H}{\partial P} + x_m \frac{\partial \mu_m^H}{\partial P} + x_s \frac{\partial \mu_s^H}{\partial P} + x_w \frac{\partial \mu_w^H}{\partial P} + \mu_c \frac{\partial x_c}{\partial P} + \mu_m \frac{\partial x_m}{\partial P} + \mu_s \frac{\partial x_s}{\partial P} + \mu_w \frac{\partial x_w}{\partial P} \quad \text{(A-29)}$$

where the chemical potential gradients with respect to pressure can be given by:

$$\left(\frac{\partial \mu_r^H}{\partial P}\right) = \bar{V}_r \quad \text{(A-30)}$$

Thus equation (A-29) can be written as:

$$\frac{\partial G_H}{\partial P} = x_c \bar{V}_c + x_s \bar{V}_s + x_m \bar{V}_m + x_w \bar{V}_w + \mu_c^H \frac{\partial x_c}{\partial P} + \mu_s^H \frac{\partial x_s}{\partial P} + \mu_m^H \frac{\partial x_m}{\partial P} + \mu_w^H \frac{\partial x_w}{\partial P} \quad \text{(A-31)}$$

The sum of the molar volumes ($\bar{V}_c$, $\bar{V}_s$, $\bar{V}_m$, $\bar{V}_w$) is in fact the total clathrate molar volume:

$$\bar{V}^{clath} = x_c \cdot \bar{V}_c + x_s \cdot \bar{V}_s + x_m \cdot \bar{V}_m + x_w \cdot \bar{V}_w \quad \text{(A-32)}$$

Using the above value of $\bar{V}^{clath}$ will reduce equation (A-31) to:

$$\frac{\partial G_H}{\partial P} = \bar{V}^{clath} + \mu_c^H \frac{\partial x_c}{\partial P} + \mu_s^H \frac{\partial x_s}{\partial P} + \mu_m^H \frac{\partial x_m}{\partial P} + \mu_w^H \frac{\partial x_w}{\partial P} \quad \text{(A-33)}$$

The mole fraction derivatives can be calculated from equation of state but there is no change under this derivative so equation (A-33) can be rewritten as:

$$\left(\frac{\partial G_H}{\partial P}\right)_{T,V,\bar{x}} = \bar{V}^{clath} \quad \text{(A-34)}$$

The free energy gradient with respect to temperature comes from the same fundamental relationship as used for the chemical potential gradient:

$$-\frac{\partial}{\partial T}\left[\frac{G}{T}\right]_{P,\vec{x}} = \frac{\bar{H}}{T^2}$$

(A-35)

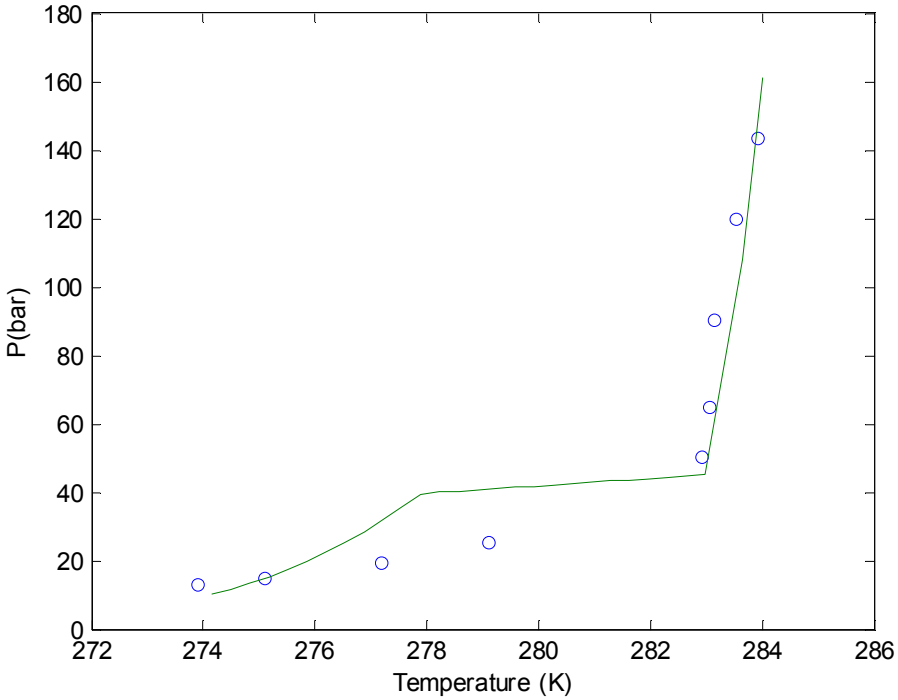

Figure 1 The estimated hydrate equilibrium for CO2 hydrate (solid line) compared to experimental data from Ng & Robinson (1985) and Larson (1985) (o).

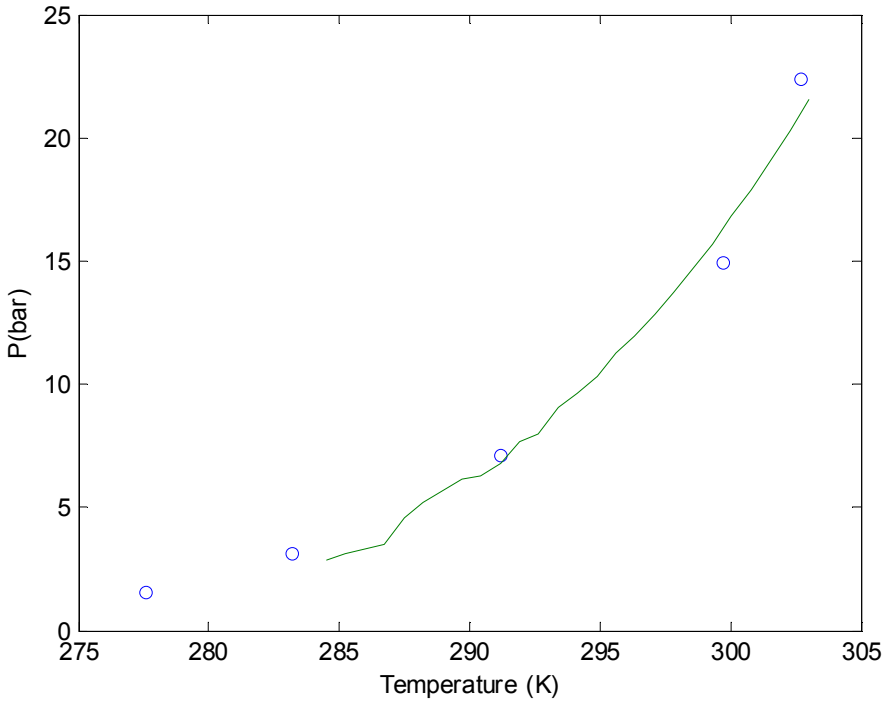

Figure 1 The estimated hydrate equilibrium curve for H2S hydrate (solid line) compared to experimental data from Bond & Russel [12].

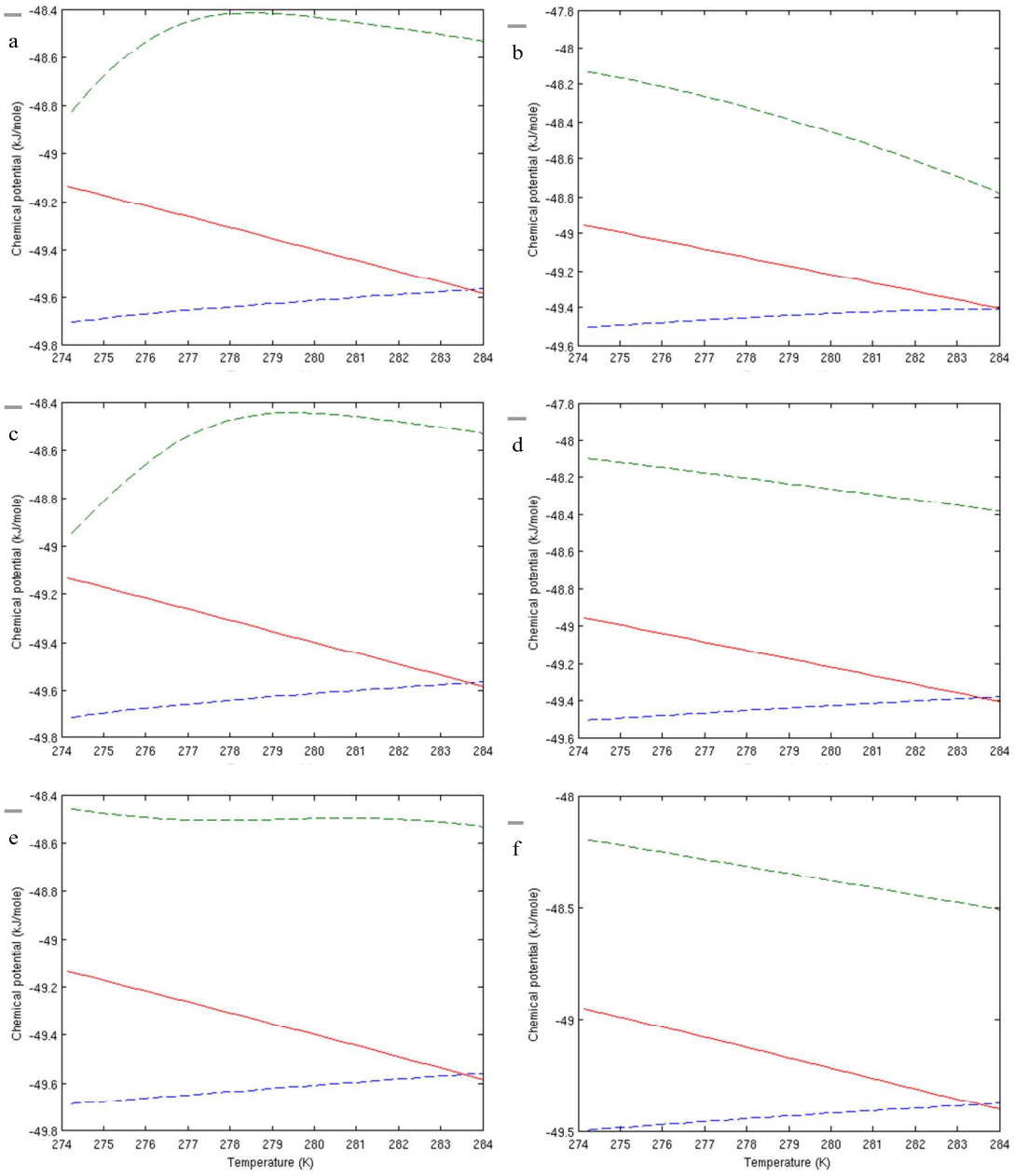

Figure 3: Chemical potentials of liquid water (solid line), water in hydrate formed from a mixture of H2S in CO2 (dashed curve at the bottom), and water in hydrate formed by the H2S alone (dashed curve at the top). Following pressures and H2S mole fractions:

(a) 100 bar, 0.001; (b) 200 bar, 0.001; (d) 100 bar, 0.003; (d) 200 bar, 0.003; (e) 100 bar, 0.025; (f) 200 bar, 0.025.

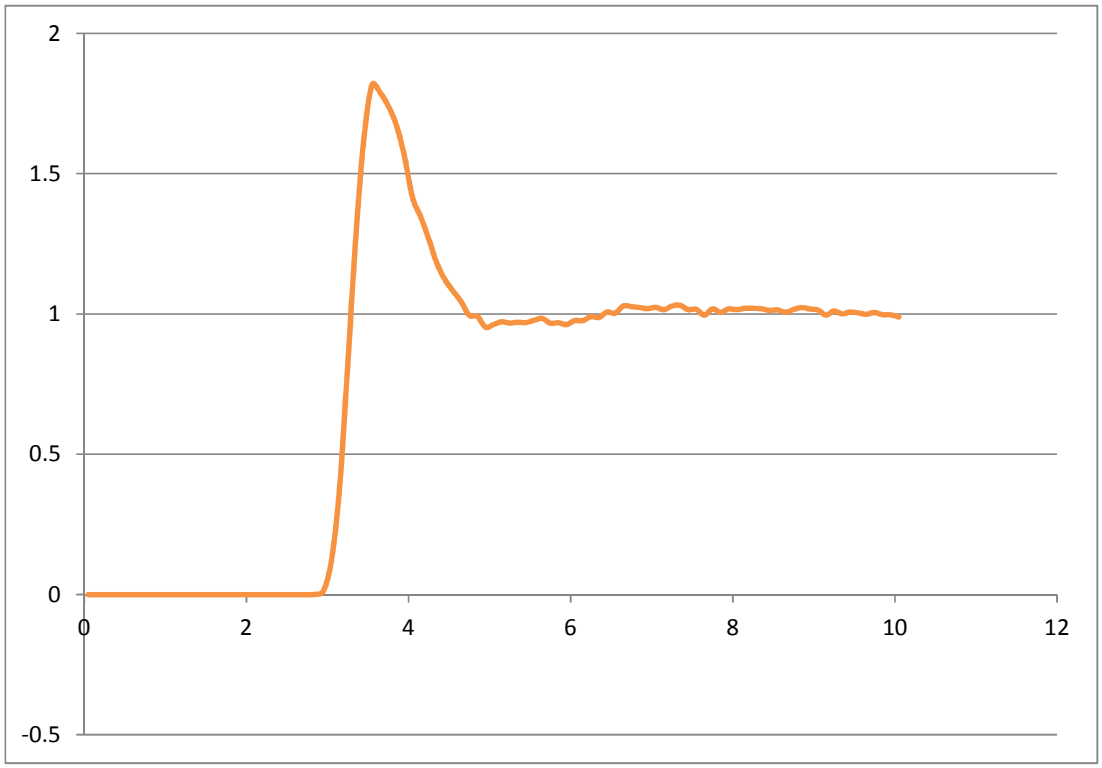

Figure 4: Radial distribution function, g(r), between sulfur and oxygen atoms for hydrogen sulfide dissolved in carbon dioxide. Temperature 274.15 K and density of 0.94802 g/cm3 corresponded to pressure of 70 atm.

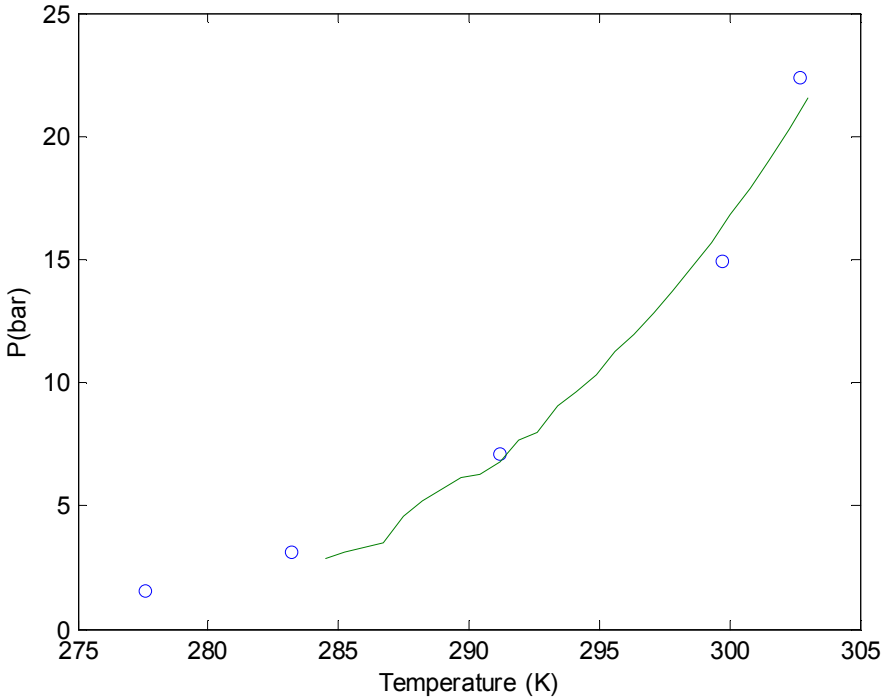

Deciding on the upper bound of water content permissible in a stream of dense carbon dioxide under pipeline transport conditions without facing the risks of hydrate formation is a complex issue. In this work, we outline and analyze ten primary routes of hydrate formation inside a rusty pipeline, with hydrogen sulfide, methane, argon, and nitrogen as additional impurities. A comprehensive treatment of equilibrium absolute thermodynamics as applied to multiple hydrate phase transitions is provided. We also discuss in detail the implications of the Gibbs phase rule that make it necessary to consider non-equilibrium thermodynamics. The analysis of hydrate risk has been revised for the dominant routes, including the one traditionally considered in industrial practice and hydrate calculators. The application of absolute thermodynamics with parameters derived from atomistic simulations lead us to several important conclusions regarding the impact of hydrogen sulfide. When present at studied concentrations below 5 mol%, the presence of hydrogen sulfide will only support the carbon-dioxide-dominated hydrate forming on the phase interface from liquid water and hydrate formers entering from the carbon dioxide phase. This is in contrast to a homogeneous hydrate nucleation and growth inside the aqueous solution bulk. Our case studies indicate that hydrogen sulfide at higher than 0.1 mol% concentration in the carbon dioxide can lead to growth of multiple hydrate phases immediately adjacent to the adsorbed water layers. We conclude that hydrate formation via water adsorption on rusty pipeline walls will be the dominant contributor to the hydrate formation risk, with initial concentration of hydrogen sulfide being the critical factor.